symmetry

MDPI

Article

MHD Stagnation Point Flow of Nanofluid on a Plate with Anisotropic Slip

Muhammad Adil Sadiq

Department of Mathematics, DCC-KFUPM, KFUPM Box 5084, Dhahran 31261, Saudi Arabia; adilsadiq@kfupm.edu.sa; Tel.: +966-598-658-229

Received: 1 January 2019; Accepted: 22 January 2019; Published: 24 January 2019

Abstract: In this article, an axisymmetric three-dimensional stagnation point flow of a nanofluid on a moving plate with different slip constants in two orthogonal directions in the presence of uniform magnetic field has been considered. The magnetic field is considered along the axis of the stagnation point flow. The governing Naiver–Stokes equation, along with the equations of nanofluid for three-dimensional flow, are modified using similarity transform, and reduced nonlinear coupled ordinary differential equations are solved numerically. It is observed that magnetic field M and slip parameter λ_1 increase the velocity and decrease the boundary layer thickness near the stagnation point. Also, a thermal boundary layer is achieved earlier than the momentum boundary layer, with the increase in thermophoresis parameter N_t and Brownian motion parameter N_b. Important physical quantities, such as skin friction, and Nusselt and Sherwood numbers, are also computed and discussed through graphs and tables.

Keywords: stagnation point flow; numerical solution; magnetic field; nanofuid

1. Introduction

The phenomenon of stagnation point flow has various uses in and aerodynamic industries. Such flows mainly compact with the movement of fluid close to the stagnated region of a rigid surface flowing in the fluid material, or retained with dynamics of fluid. Stagnation point has been studied by many researchers in the past because of its wide range of applications in engineering. Initially, stagnation point flow was analyzed by Hiemenz in 1911. He studied the two-dimensional stagnation point flow on a stationary plate. Stagnation point flow applications include cooling of electronic devices by fans, cooling of nuclear reactors, polymer extrusion, wire drawing, drawing of plastic sheets, and many hydrodynamic processes in engineering applications. Stagnation point flow possesses much physical significance, as it is used to calculate the velocity gradients and the rate of heat and mass transfer abutting to stagnation area of frames in high-speed flows, cooling of transpiration, rustproof designs of bearings, etc.

Recently, Borrelli et al. [1] deliberated over the impact of buoyancy on three-dimensional (3D) stagnation point flow. They stated that the buoyancy forces tend to favor an opposite flow. Later, Lok et al. [2] expanded on the work of Weidman [3] with buoyancy forces. They observed the discrete results for free convection and forced convection due to a singularity rising in the convection term. Steady oblique stagnation point flow of a viscous fluid was studied by Grosan et al. [4]. They solved the nonlinear coupled differential equation numerically using the Runge–Kutta method. It is observed that the location of the stagnation point depends strongly on the value of the shear parameter and magnetic parameter. Wang [5–7] discussed the three-dimensional stagnation flow in the absence of MHD and nanofluids on a flat plate, shrining disk, and rotating disk. Two-dimensional (2D) stagnation flow was discussed by Nadeem et al. [8] using HAM on a stretchable surface.

A fluid, heated by electric current in the presence of strong magnetic field, for example crystal growth in melting, has relevance in manufacturing industries. During the fluid motion, the association of electric current and magnetic field produces a divergence of Lorentz forces. This phenomenon prevents the convective motion of fluid and heat transfer characteristic changes accordingly. Ariel [9] investigated the flow near the stagnation point numerically for small magnetic fields; for large magnetic numbers, the perturbation technique was used. Raju and Sundeep [10] proved that with an increase in the magnetic number, there is an increase in the heat and mass transfer rates. They studied numerically the MHD flow of non-Newtonian fluid over a rotating cone or plate.

Generally, the size of nanoparticles is (1–100 nm). Currently, nanofluids are used for drug delivery in infected areas of the human body. Self-propagating objects containing drugs are used to remove blood clots in sensitive areas such as the brain, eye, heart, etc. Kleinstreuer [11] discussed the drug delivery system in humans at normal body temperature under the influence of some physical parameters such as nanoparticle length, artery diameter, and velocity of fluid. Recently, a mathematical model of nanofluid was developed by Choi [12]. Later, a contribution to heat transfer analysis in nanofluid was made by Buongiorno [13]. His mathematical model dealt with the non-homogeneous model for transport phenomena and heat transfer in nanofluids with applications to turbulence. Saleem et al. [14] discussed the effects of Brownian diffusion and thermophoresis on non-Newtonian fluid models, using HAM in the domain of a vertical rotating cone. Bachok et al. [15] studied the three-dimensional stagnation flow of a viscous fluid numerically, analyzed the velocity and heat transfer for different physical parameters, and compared three nanoparticles, namely C_u, Al_2O_3, T_iO_3. In [16] Ellahi et al. explored the heat and mass transfer of non-Newtonian fluid in an annulus in a porous medium using HAM. Recently, Sheikholeslami et al. [17] studied the effects of thermal radiation on steady viscous nanofluid in the presence of MHD numerically. Khan [18] explored Brownian diffusion and thermophoresis on stagnation point flow. He considered dual solutions for shrinking/stretching parameters and heat transfer in the presence of buoyancy forces on a stretchable surface. Mustafa et al. [19] investigated 3D nanofluid flow and heat transfer in two opposite directions on a plane horizontal stretchable surface. Thermal and momentum boundary layers were discussed using physical parameters such as Brownian motion and thermophoretic forces. Some more useful studies related to nanofluids can be found in [20–29].

In this article, an axisymmetric 3D stagnation point flow of a nanofluid on a moving plate with different slip constants in two orthogonal directions in the presence of uniform magnetic field has been considered and solved numerically.

2. Mathematical Formulation

Consider a stagnation point flow of a nanofluid over a plate with anisotropic slip in a Cartesian coordinate system, so that the x-axis is taken along the corrugations of plates, the y-axis is normal to the corrugations, and the z-axis is considered with the axis of stagnation flow. The velocities of the moving plate are (u, v) in (x, y) directions, respectively. A constant magnetic field is applied perpendicular to the corrugation along the axis of the stagnation flow in such a way that the magnetic Reynolds number is small. According to Wang [5], the potential flow far from the plate is defined as:

$$uu_x + vu_y + wu_z = -\frac{p_x}{\rho} + \nu\left(u_{xx} + u_{yy} + u_{zz}\right) - \frac{B_0^2}{\rho}u, \tag{1}$$

$$uv_x + vv_y + wv_z = -\frac{p_y}{\rho} + \nu\left(v_{xx} + v_{yy} + v_{zz}\right) - \frac{B_0^2}{\rho}v, \tag{2}$$

$$uw_x + vw_y + ww_z = -\frac{p_z}{\rho} + \nu\left(w_{xx} + w_{yy} + w_{zz}\right), \tag{3}$$

$$
\begin{aligned}
u\frac{\partial T}{\partial x}+v\frac{\partial T}{\partial y}+w\frac{\partial T}{\partial z} &= \alpha_m\left(\frac{\partial^2 T}{\partial x^2}+\frac{\partial^2 T}{\partial y^2}+\frac{\partial^2 T}{\partial z^2}\right)\\
&+ \frac{(\rho C)_p}{(\rho C)_f}\left[D_B\left(\frac{\partial C}{\partial x}\frac{\partial T}{\partial x}+\frac{\partial C}{\partial y}\frac{\partial T}{\partial y}+\frac{\partial C}{\partial z}\frac{\partial T}{\partial z}\right)\right]\\
&+ \frac{D_T}{T_\infty}\left[\left(\frac{\partial T}{\partial x}\right)^2+\left(\frac{\partial T}{\partial y}\right)^2+\left(\frac{\partial T}{\partial z}\right)^2\right], \qquad (4)\\
u\frac{\partial C}{\partial x}+v\frac{\partial C}{\partial y}+w\frac{\partial C}{\partial z} &= D_B\left[\frac{\partial^2 C}{\partial x^2}+\frac{\partial^2 C}{\partial y^2}+\frac{\partial^2 C}{\partial z^2}\right]\\
&+ \frac{D_T}{T_\infty}\left[\frac{\partial^2 T}{\partial x^2}+\frac{\partial^2 T}{\partial y^2}+\frac{\partial^2 T}{\partial z^2}\right]. \qquad (5)
\end{aligned}
$$

and the boundary conditions are:

$$
\begin{aligned}
&u-U=N_1\mu\frac{\partial u}{\partial z} \quad ,v-V=N_2\mu\frac{\partial v}{\partial z},\ \ T=T_w,\ \ C=C_\infty \quad at \quad z=0,\\
&u\to ax, v\to ay, T\to T_\infty, C\to C_\infty \quad at \quad z\to\infty. \qquad (6)
\end{aligned}
$$

where (u,v) are the velocity components in the (x,y) directions, ν is the kinematic viscosity, T is the temperature, α_m is the thermal diffusivity, C is the volume of nanoparticles, $(\rho C)_p$ is the effective heat capacity of nanoparticles, $(\rho C)_f$ is the heat capacity of fluid, D_B is the Brownian diffusion coefficient and D_T is the thermophoretic diffusion coefficient. For the non-dimensionalization, we use the following similarity variables:

$$
\begin{aligned}
u &= axf^{'}(\eta)+Uh(\eta),\\
v &= ayg^{'}(\eta)+Vk(\eta),\\
w &= -\sqrt{av}\ [f(\eta)+g(\eta)]. \qquad (7)
\end{aligned}
$$

where $\eta=\sqrt{a/\nu}\ z$. Using Equation (7) in Equations (5) and (6) finally we get:

$$
\begin{aligned}
f^{'''}+f^{''}(f+g)-(f^{'})^2-M^2f^{'} &= -(1+M^2) \qquad (8)\\
g^{'''}+g^{''}(f+g)-(g^{'})^2-M^2g^{'} &= -(1+M^2) \qquad (9)\\
h^{''}+h^{'}(f+g)-hf^{'}-M^2h &= 0 \qquad (10)\\
k^{''}+k^{'}(f+g)-kg^{'}-M^2k &= 0 \qquad (11)\\
\theta^{''}+P_r(f+g)\theta^{'}+P_r\left[N_t\theta^{'}\phi^{'}+N_b(\theta^{'})^2\right] &= 0 \qquad (12)\\
\phi^{''}+S_c(f+g)\phi^{'}+\frac{N_t}{N_b}\theta^{''} &= 0. \qquad (13)
\end{aligned}
$$

and boundary conditions are:

$$
\begin{aligned}
&f^{'}(0)=\lambda_1 f^{''}(0),\ g^{'}(0)=\lambda_2 g^{''}(0),\ h(0)=1+\lambda_1 h^{'}(0),\ k(0)=1+\lambda_2 k^{'}(0),\ f(0)=0, g(0)=0,\\
&f^{'}(\infty)\to 1,\ g^{'}(\infty)\to 1,\ h(\infty)\to 1,\ k(\infty)\to 1,\ \theta(0)=1,\ \theta(\infty)\to 0,\ \phi(0)=1,\ \phi(\infty)\to 0. \qquad (14)
\end{aligned}
$$

here λ_1 and λ_2 are the slip parameters, P_r the prantle number, S_c the Schmidt number, N_t and N_b are thermophoresis parameter, Brownian motion parameters, respectively.

The expression for the skin friction coefficient, the local Nusselt number, and Sherwood number for second-grade fluid are defined as:

$$
Re_x^{1/2}\ C_f=f^{''}(0),\ \ Nu_x\ Re_x^{-1/2}=-\theta^{'}(0),\ \ Sh_x\ Re_x^{-1/2}=-\varphi^{'}(0), \qquad (15)
$$

where $Re_x = \frac{U_w x}{\nu}$ is the local Reynolds number. The solution of above coupled nonlinear differential equations are found numerically and discussed in the following section.

3. Result and Discussion

A system of nonlinear ordinary differential Equations (8)–(13) subject to the boundary conditions of Equation (14) are solved numerically using the Richardson extrapolation enhancement method. Richardson extrapolation is generally faster, and capable of handling BVP systems with unknown parameters. The values of these parameters can be determined under the presence of a sufficient number of boundary conditions. The solutions are discussed through graphs from Figures 1–10, and values of physical quantities, such as skin friction and Nusselt and Sherwood numbers, are presented in Tables 1–3.

Figures 1 and 2 show the variation of velocity profile f' and g' against η for different values of magnetic field M and slip parameter λ_1. It was observed that increasing in the values of M and λ_1 causes increase in the velocity profile, while boundary layer thickness reduces. Thus, these parameters cause a reduction in the momentum boundary layer. Analysis shows that increasing the values of these parameters to a sufficiently large level shows the monotonic behavior of velocity throughout the whole domain. Figures 3 and 4 shows the opposite behavior of h and k with the increment of M and λ_1, such that with the increase in value of these parameters, h and k decreases.

The temperature profile for the nanofluid against different values of thermophoresis parameter N_t and Brownian motion parameter N_b are plotted in Figures 5 and 6. As the temperature increase within the boundary layer, the values of these parameters increase. The thermal boundary layer is achieved earlier than the momentum boundary layer. The variation of nanoconcentration for different values of Schmidt number S_c and N_t is presented in Figures 7 and 8, respectively. It is observed that nanoconcentration ϕ decreases as the increase in S_c and boundary layer thickness decreases. Also, with the increase in N_t, the nanoconcentration decreases. Figures 9 and 10 show the velocity profile for different values of magnetic parameter $M = 0$ and for $M = 2$. It is observed that in the absence of magnetic parameter M, the boundary layer thickness is larger than while M is present. $M = 0$ in Figures 11 and 12 represents the results of Wang [5]. The slip parameter ratio can be defined as $\gamma = \frac{\lambda_2}{\lambda_1}$. Figures 13 and 14 describe the $f'(\eta), g'(\eta)$ for $\gamma = 0.5$. The range of γ varies from 0.2 to 10. $\gamma = 1$ represents the isotropic case where $f'(\eta) = g'(\eta)$ and $h(\eta) = k(\eta)$.

Table 1 shows local Nusselt number Nu_x and local Sherwood number Sh_x for the variation of P_r and thermophoresis parameter N_b. Here we see that with the increase of P_r, the local Nusselt number decreases, while local Sherwood number gives opposite results, meaning Sh_x increases. Moreover, with the increase of N_b, the results are again the opposite for Nu_x and Sh_x. Table 2 shows local Nusselt number and local Sherwood number for variations of slip parameter λ_1 and Brownian motion Nb. Here it is observed that with the increase of λ_1 both Nusselt number and local Sherwood number increase. Table 3 shows the skin friction coefficient C_f for different values of λ_1 and magnetic parameter M. Note that with the increment in λ_1, the value of skin friction decreases. A high value of M gives larger values of skin friction.

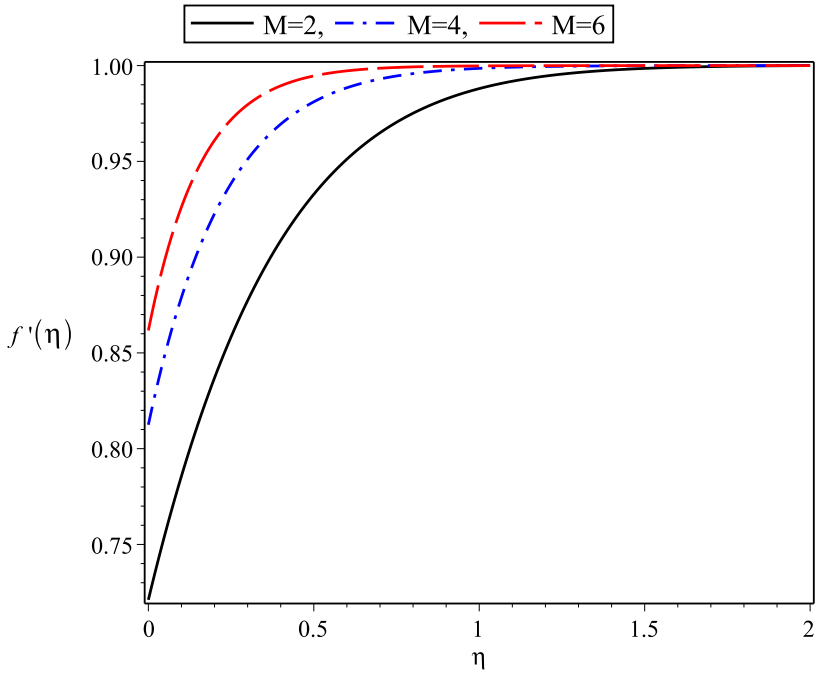

Figure 1. Variation of $f'(\eta)$ for different M.

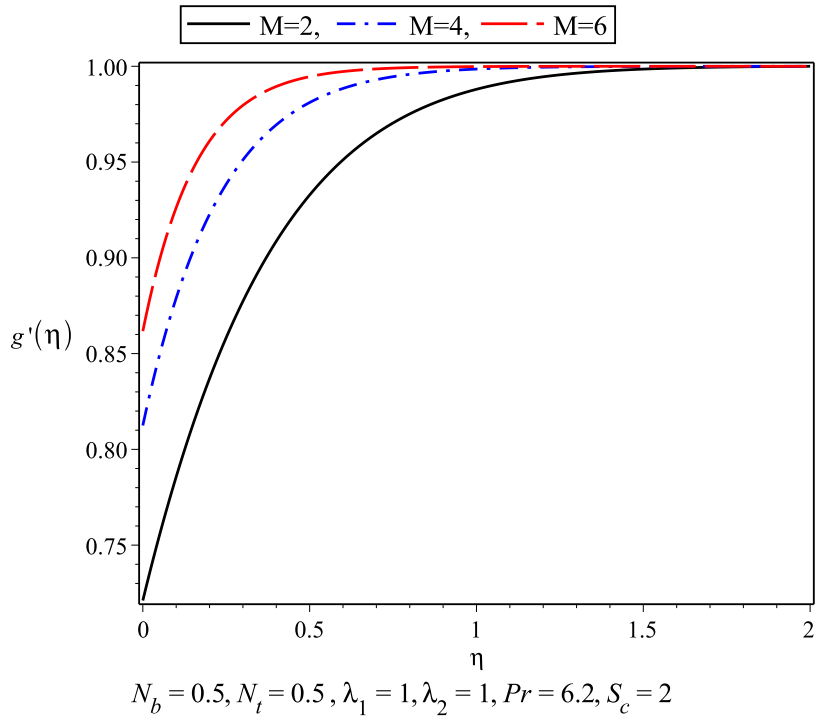

Figure 2. Variation of $g'(\eta)$ for different M.

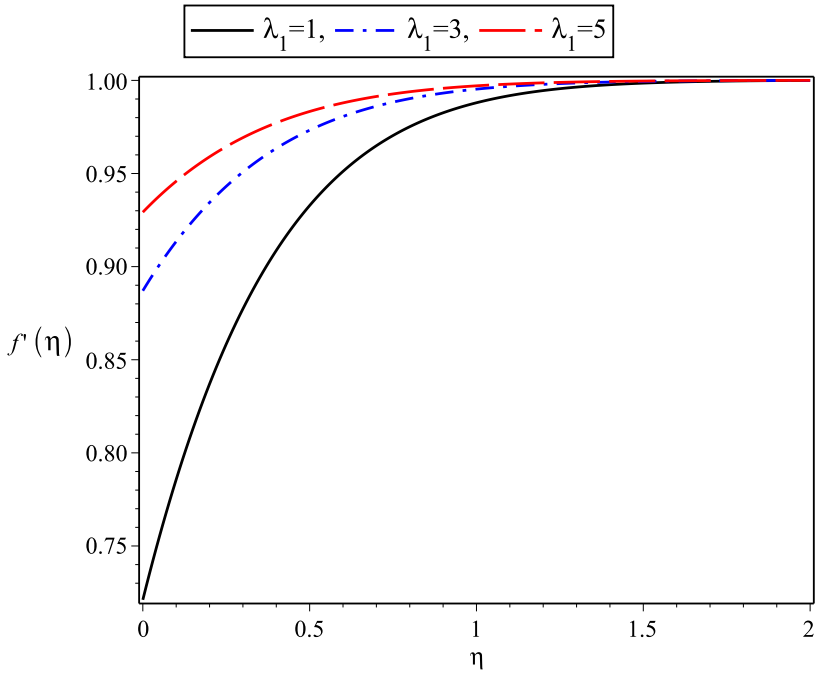

Figure 3. Variation of $f'(\eta)$ for different λ_1.

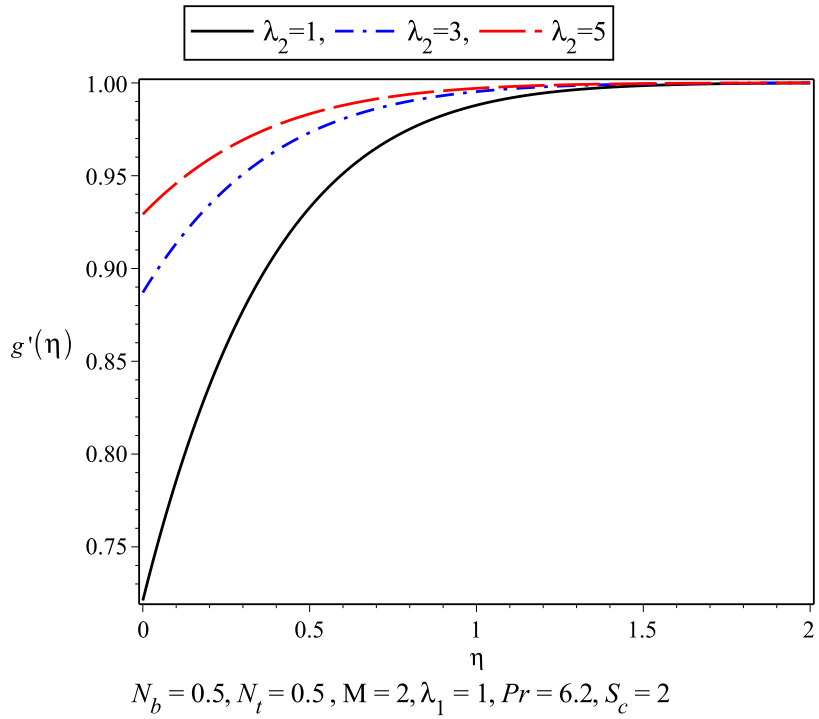

Figure 4. Variation of $g'(\eta)$ for different λ_2.

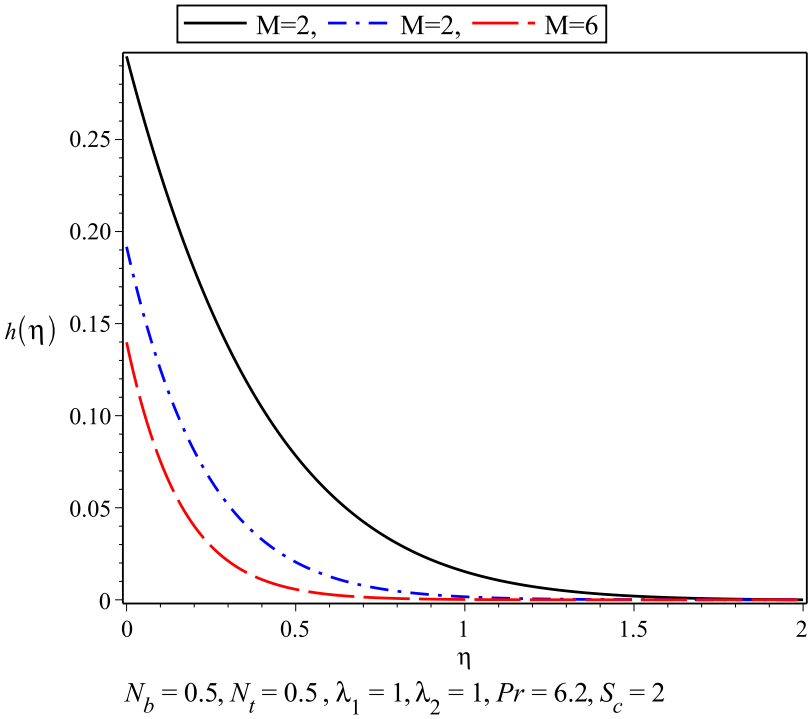

Figure 5. Variation of $h(\eta)$ for different M.

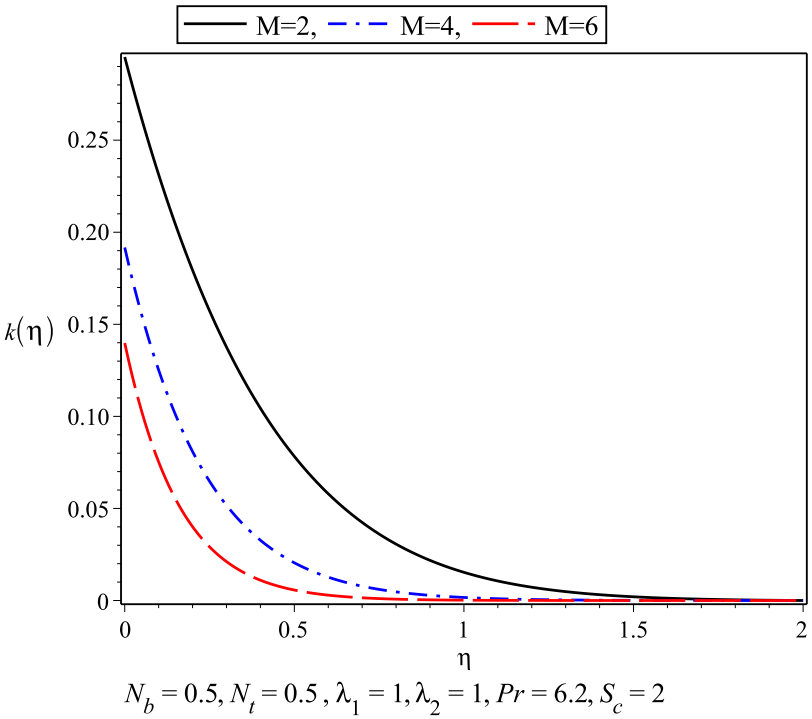

Figure 6. Variation of $k(\eta)$ for different M.

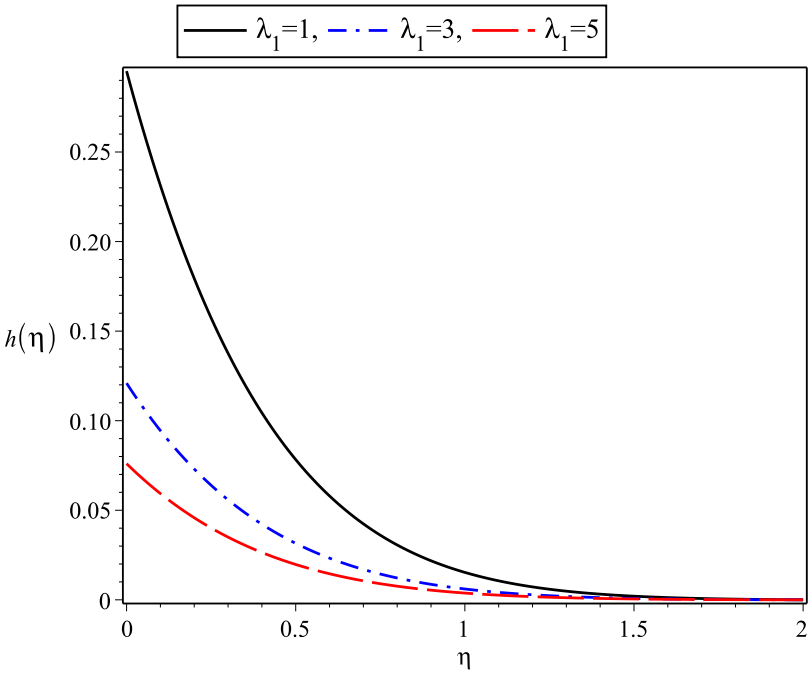

Figure 7. Variation of $h(\eta)$ for different λ_1.

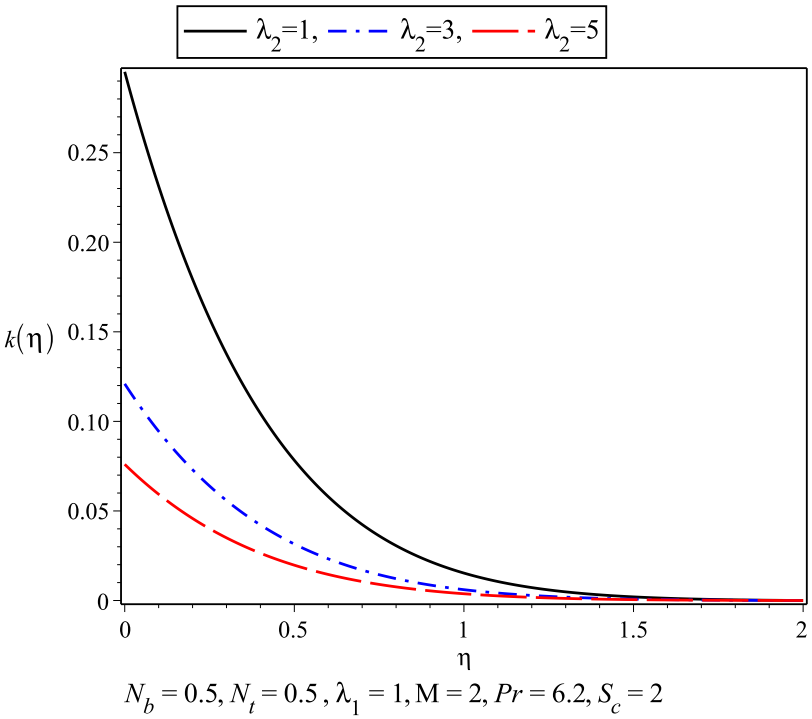

Figure 8. Variation of $k(\eta)$ for different λ_2.

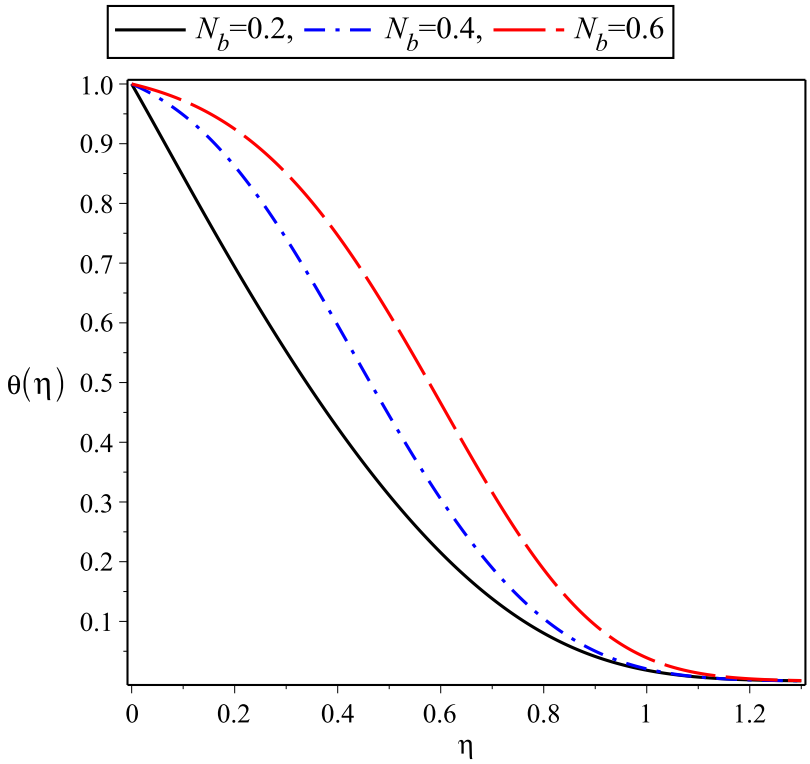

Figure 9. Variation of $\theta(\eta)$ for different N_b.

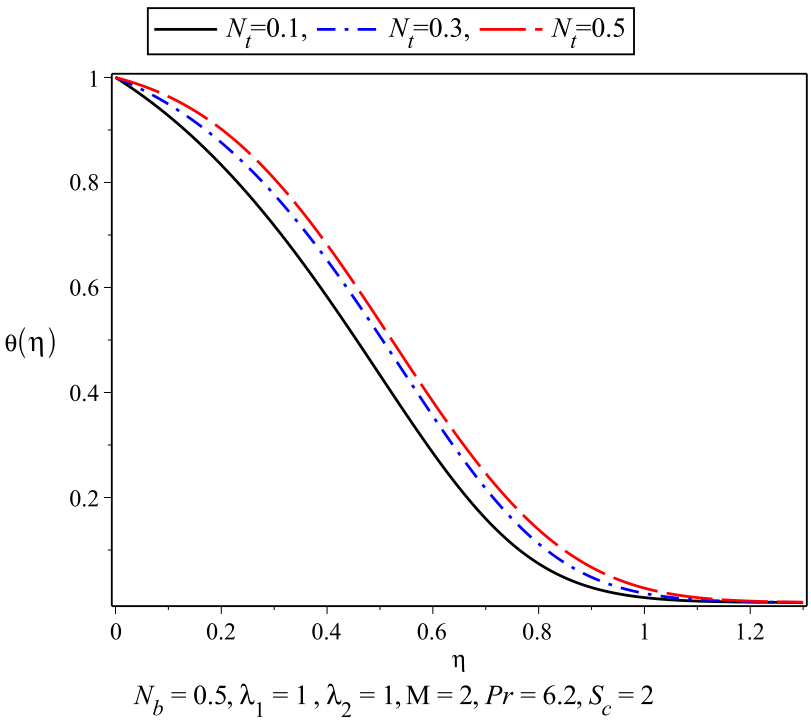

Figure 10. Variation of $\theta(\eta)$ for different N_t.

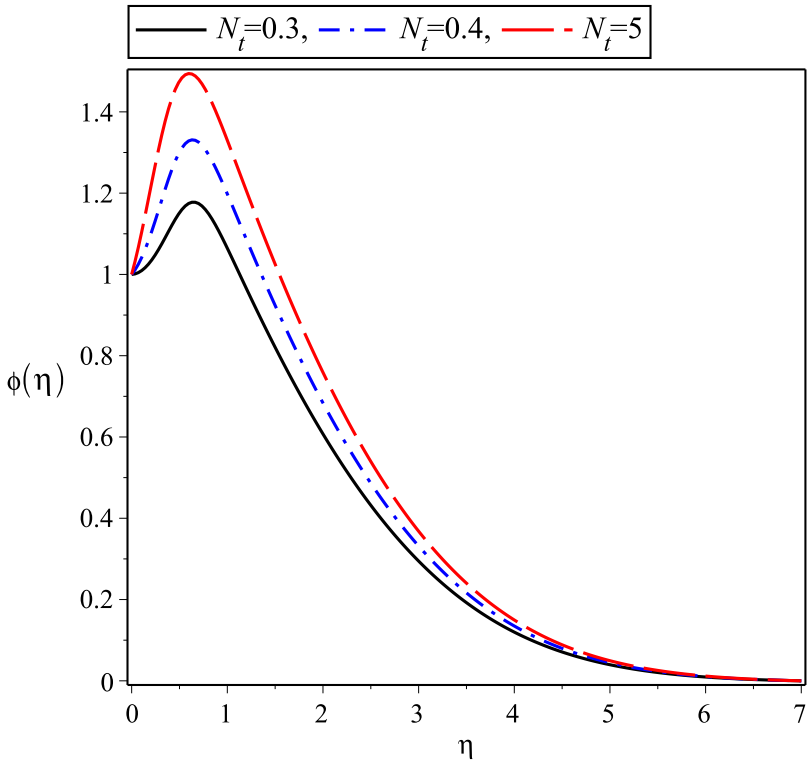

Figure 11. Variation of $\phi(\eta)$ for different N_t.

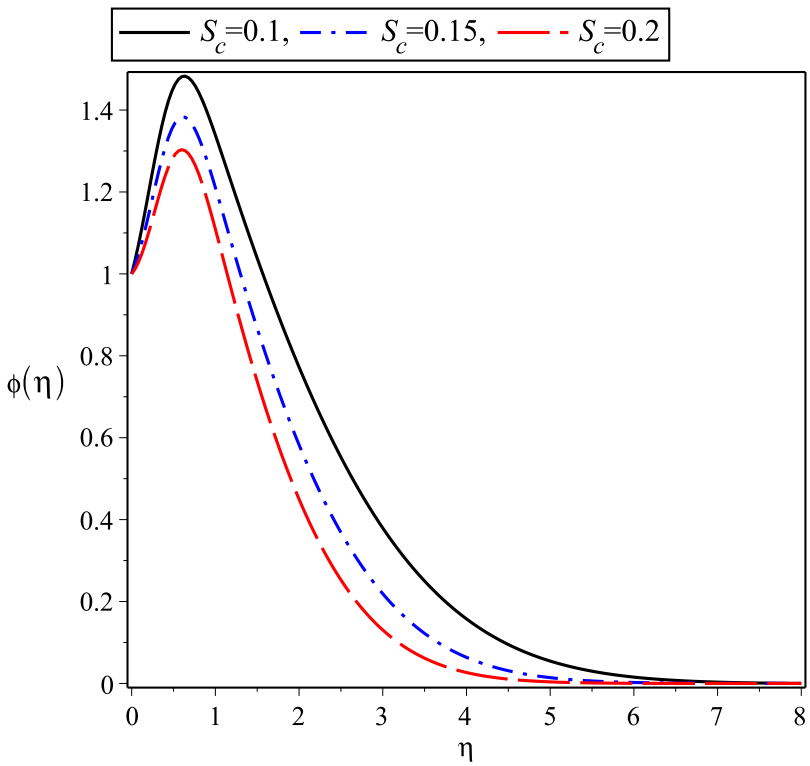

Figure 12. Variation of $\phi(\eta)$ for different S_c.

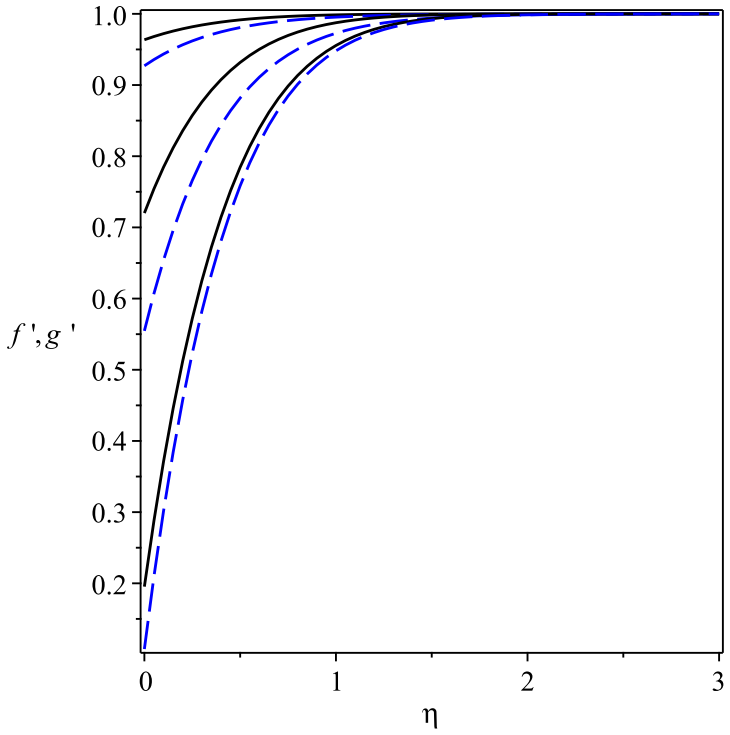

Figure 13. $f'(\eta)$ solid curves and $g'(\eta)$ dashed curves for $\gamma = \frac{\lambda_2}{\lambda_1} = 0.5$. From top: $\lambda_1 = 10, 1, 0.1$.

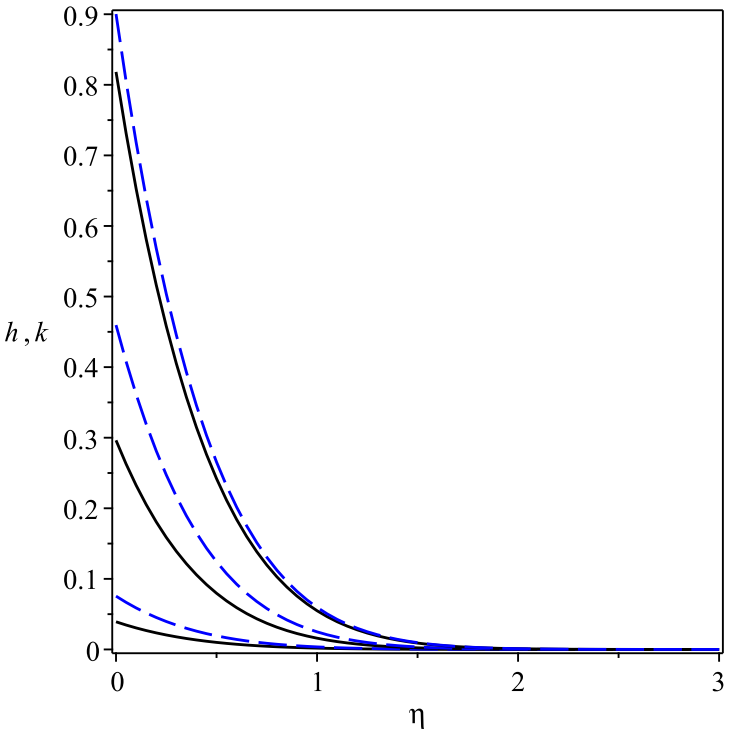

Figure 14. $h(\eta)$ solid curves and $k(\eta)$ dashed curves for $\gamma = \frac{\lambda_2}{\lambda_1} = 0.5$. From top: $\lambda_1 = 10, 1, 0.1$.

Table 1. Variation of Local Nusselt number Nu_x and Sherwood number Sh_x for different N_b and P_r.

$\lambda_1 = 1, \lambda_2 = 1, S_c = 2, M = 2, N_t = 0.5$						
	$N_b = 0.1$		$N_b = 0.3$		$N_b = 0.5$	
P_r	Nu_x	Sh_x	Nu_x	Sh_x	Nu_x	Sh_x
5.5	0.67084	1.47332	0.45477	1.58078	0.30641	1.77542
5.6	0.66527	1.47440	0.44833	1.58438	0.29987	1.78168
5.7	0.65976	1.47546	0.44197	1.58792	0.29346	1.78781
5.8	0.65431	1.47651	0.43570	1.59139	0.28716	1.79381
5.9	0.64890	1.47754	0.42950	1.59481	0.28098	1.79968
6.0	0.64355	1.47856	0.42343	1.59816	0.27492	1.80543
6.1	0.63826	1.47956	0.41742	1.60145	0.26897	1.81105
6.2	0.63302	1.48055	0.41150	1.60468	0.26314	1.81655
6.3	0.62784	1.48152	0.40566	1.60785	0.25742	1.82192
6.4	0.62272	1.48248	0.39992	1.61096	0.25181	1.82718
6.5	0.61766	1.48342	0.39425	1.61401	0.24631	1.83232

Table 2. Variation of Local Nusselt number Nu_x and Sherwood number Sh_x for different M and λ_1.

$\lambda_2 = 1, S_c = 2, N_b = 0.5, N_t = 0.5, P_r = 6.2$						
	$M = 2$		$M = 4$		$M = 6$	
λ_1	Nu_x	Sh_x	Nu_x	Sh_x	Nu_x	Sh_x
0.5	0.25129	1.78860	0.27363	1.85616	0.28527	1.88559
0.6	0.25465	1.79657	0.27603	1.86128	0.28698	1.88892
0.7	0.25737	1.80301	0.27791	1.86529	0.28829	1.89145
0.8	0.25962	1.80831	0.27943	1.86850	0.28933	1.89350
0.9	0.26152	1.81276	0.28068	1.87114	0.29018	1.89513
1.0	0.26314	1.81655	0.28172	1.87335	0.29087	1.89648
1.1	0.26453	1.81980	0.28261	1.87522	0.29146	1.89762
1.2	0.26575	1.82263	0.28337	1.87683	0.29196	1.89859
1.3	0.26682	1.82511	0.28403	1.87822	0.29239	1.89942
1.4	0.26776	1.82731	0.28461	1.87944	0.29277	1.90015
1.5	0.26861	1.82926	0.28513	1.88052	0.29310	1.90079

Table 3. Variation of Skin friction coefficient for different M and λ_1.

$\lambda_2 = 1, S_c = 2, N_b = 0.5, N_t = 0.5, P_r = 6.2$			
	$M = 2$	$M = 4$	$M = 6$
λ_1	C_f	C_f	C_f
0.5	1.12177	1.36687	1.51354
0.6	1.00998	1.20285	1.31469
0.7	0.91823	1.07391	1..16200
0.8	0.84163	0.96991	1.04108
0.9	0.77675	0.88425	0.94294
1.0	0.72109	0.81248	0.86171
1.1	0.67283	0.75148	0.79336
1.2	0.63060	0.69899	0.73505
1.3	0.59334	0.65335	0.68473
1.4	0.56022	0.61330	0.64086
1.5	0.53059	0.57788	0.60227

4. Conclusions

The current paper investigated the effects of uniform magnetic field of axisymmetric three-dimensional stagnation point flow of a nanofluid on a moving plate with different slip constants.

The governing equations were made dimensionless and then solved using the Richardson extrapolation enhancement method. The following are the findings of the above work:

- An increase in the magnetic field M and slip parameter λ_1 causes an increase in the velocity profile and decrease in the boundary layer thickness near the stagnation point.
- It is observed that in the absence of magnetic parameter M the boundary layer thickness is larger than while M is present.
- The thermal boundary layer increases with an increase in the thermophoresis parameter N_t and Brownian motion parameter N_b. It is observed that the thermal boundary layer is achieved earlier compared to the momentum boundary layer.
- It is observed that with the increase in S_c and N_t the nanoconcentration ϕ decreases and vice versa.

Funding: The author wishes to express his thanks for financial support received from King Fahd University of Petroleum and Minerals.

Acknowledgments: The author wishes to express his thanks to King Fahd University of Petroleum and Minerals and reviewers to improve the manuscript.

Conflicts of Interest: The author declares that there is no conflict of interest.

Abbreviations

The following abbreviations are used in this manuscript:

(u, v)	velocity Components
ν	kinematic viscosity
N_1, N_2	slip coefficient
T	temperature
α_m	thermal diffusivity
C	volume of nano particles
$(\rho C)_f$	heat capacity of fluid
D_B	Brownian diffusion coefficient
D_T	thermophoretic diffusion coefficient
λ_1, λ_2	slip parameters
N_t	thermophoresis parameter
N_b	browning motion parameter
C_f	skin friction coefficient
Nu_x	local Nusselt number
Sh_x	Sherwood number
Re_x	local Reynolds number
S_c	Schmidt number
Pr	prantle number
γ	ratio of slip parameters
ϕ	nano concentration
M	magnetic parameter

References

1. Borrelli, A.; Giantesio, G.; Patria, M.C. Numerical simulations of three-dimensional MHD stagnation-point flow of a micropolar fluid. *Comput. Math. Appl.* **2013**, *66*, 472–489. [CrossRef]
2. Lok, Y.Y.; Amin, N.; Pop, I. Non-orthogonal stagnation point flow towards a stretching shee. *Int. J. Non Linear Mech.* **2006**, *41*, 622–627. [CrossRef]
3. Tilley, B.S.; Weidman, P.D. Oblique two-fluid stagnation-point flow. *Eur. J. Mech. B Fluids* **1998**, *17*, 205–217. [CrossRef]
4. Grosan, T.; Pop, I.; Revnic, C.; Ingham, D.B. Magnetohydrodynamic oblique stagnation-point flow. *Meccanica* **2009**, *44*, 565. [CrossRef]

5. Wang, C.Y. Stagnation flow on a plate with anisotropic slip. *Eur. J. Mech. B Fluids* **2013**, *38*, 73–77. [CrossRef]
6. Wang, C.Y. Off-centered stagnation flow towards a rotating disc. *Int. J. Eng. Sci.* **2008**, *46*, 391–396. [CrossRef]
7. Wang, C.Y. Stagnation flow towards a shrinking sheet. *Int. J. Non Linear Mech.* **2008**, *43*, 377–382. [CrossRef]
8. Nadeem, S.; Hussain, A.; Khan, M. HAM solutions for boundary layer flow in the region of the stagnation point towards a stretching sheet. *Commun. Nonlinear Sci. Numer. Simul.* **2010**, *15*, 475–481. [CrossRef]
9. Ariel, P.D. Hiemenz flow in hydromagnetics. *Acta Mech.* **1994**, *103*, 31–43. [CrossRef]
10. Raju, C.S.; Sandeep, N. Heat and mass transfer in MHD non-Newtonian bio-convection flow over a rotating cone/plate with cross diffusion. *J. Mol. Liq.* **2016**, *215*, 115–126. [CrossRef]
11. Kleinstreuer, C.; Li, J.; Koo, J. Microfluidics of nano-drug delivery. *Int. J. Heat Mass Trans.* **2008**, *51*, 5590–5597. [CrossRef]
12. Choi, S.U.S. Enhancing thermal conductivity of fluids with nanoparticles. *ASME Publ. Fed* **1995**, *231*, 99–106.
13. Buongiorno, J. Convective transport in nanofluids. *J. Heat Transf.* **2006**, *128*, 240–250. [CrossRef]
14. Nadeem, S.; Saleem, S. Analytical study of third grade fluid over a rotating vertical cone in the presence of nanoparticles. *Int. J. Heat Mass Transf.* **2015**, *85*, 1041–1048. [CrossRef]
15. Bachok, N.; Ishak, A.; Nazar, R.; Pop, I. Flow and heat transfer at a general three-dimensional stagnation point in a nanofluid. *Phys. B Condens. Matter* **2010**, *405*, 4914–4918. [CrossRef]
16. Ellahi, R.; Aziz, S.; Zeeshan, A. Non Newtonian nanofluids flow through a porous medium between two coaxial cylinders with heat transfer and variable viscosity. *J. Porous Media* **2013**, *16*, 205–216. [CrossRef]
17. Sheikholeslami, M.; Ganji, D.; Javed, M.Y.; Ellahi, R. Effect of thermal radiation on nanofluid flow and heat transfer using two phase model. *J. Magn. Magn. Mater.* **2015**, *374*, 36–43. [CrossRef]
18. Makinde, O.D.; Khan, W.A.; Khan, Z.H. Buoyancy effects on MHD stagnation point flow and heat transfer of a nanofluid past a convectively heated stretching/shrinking sheet. *Int. J. Heat Mass Transf.* **2013**, *62*, 526–533. [CrossRef]
19. Junaid Ahmad Khan , M.; Mustafa, T.; Hayat, A.; Alsaedi, A. Three-dimensional flow of nanofluid over a non-linearly stretching sheet: An application to solar energy. *Int. J. Heat Mass Transf.* **2015**, *86*, 158–164. [CrossRef]
20. Upadhya, M.; Mahesha, S.; Raju, C.S.K. Unsteady Flow of Carreau Fluid in a Suspension of Dust and Graphene Nanoparticles With Cattaneo–Christov Heat Flux. *J. Heat Transf.* **2018**, *140*, 092401. [CrossRef]
21. Li, Z.; Sheikholeslami, M.; Ahmad Shafee, S.; Ali J Chamkha, S. Effect of dispersing nanoparticles on solidification process in existence of Lorenz forces in a permeable media. *J. Mol. Liq.* **2018**, *266*, 181–193. [CrossRef]
22. Raju, C.S.K.; Saleem, S.; Mamatha, S.U. Iqtadar Hussain, Heat and mass transport phenomena of radiated slender body of three revolutions with saturated porous: Buongiorno's model. *Int. J. Therm. Sci.* **2018**, *132*, 309–315. [CrossRef]
23. Ram, P.; Kumar, A. Analysis of Heat Transfer and Lifting Force in a Ferro-Nanofluid Based Porous Inclined Slider Bearing with Slip Conditions. *Nonlinear Eng.* **2018**. [CrossRef]
24. Soomro, F.A.; Hammouch, Z. Heat transfer analysis of CuO-water enclosed in a partially heated rhombus with heated square obstacle. *Int. J. Heat Mass Transf.* **2018**, *118*, 773–784.
25. Hayat, T.; Qayyum, S.; Alsaedi, A.; Ahmad, B. Results in Physics, Significant consequences of heat generation/absorption and homogeneous-heterogeneous reactions in second grade fluid due to rotating disk. *Results Phys.* **2018**, *8*, 223–230. [CrossRef]
26. Hussain, S.; Aziz, A.; Aziz, T.; Khalique, C.M. Slip Flow and Heat Transfer of Nanofluids over a Porous Plate Embedded in a Porous Medium with Temperature Dependent Viscosity and Thermal Conductivity. *Appl. Sci.* **2016**, *6*, 376. [CrossRef]
27. Anuar, N.; Bachok, N.; Pop, I. A Stability Analysis of Solutions in Boundary Layer Flow and Heat Transfer of Carbon Nanotubes over a Moving Plate with Slip Effect. *Energies* **2018**, *11*, 3243. [CrossRef]
28. Fetecau, C.; Vieru, D.; Azhar, W.A. Natural Convection Flow of Fractional Nanofluids Over an Isothermal Vertical Plate with Thermal Radiation. *Appl. Sci.* **2017**, *7*, 247. [CrossRef]

29. Khan, N.S.; Gul, T.; Islam, S.; Khan, I.; Alqahtani, A.M.; Alshomrani, A.S. Alqahtani and Ali Saleh Alshomrani, Magnetohydrodynamic Nanoliquid Thin Film Sprayed on a Stretching Cylinder with Heat Transfer. *Appl. Sci.* **2017**, *7*, 271. [CrossRef]